A layer-stripping inversion method employing a causality based imaging condition

H. Poot *, J.T. Fokkema *, C.P.A. Wapenaar *
* *Section of Applied Geophysics and Petrophysics, Delft University of Technology*

ABSTRACT

A layer-stripping inversion method is proposed here, based on Rayleigh's reciprocity theorem. Two states are defined, both in a configuration consisting of two half-spaces. The upper half-space (the background medium) is characterized by a constant acoustic wave speed, the lower half-space is inhomogeneous. The first state is the state as described by the measured pressure and velocity fields. In the second state a thin layer from the top of the lower half-space is replaced by a layer with the background medium velocity. Application of the reciprocity theorem leads to two basic equations. The first equation describes the propagation of the pressure field in the first state through the layer, which is to be replaced. The second equation describes the field after this layer has been replaced (the second state) in terms of the fields in the first state. An imaging condition was derived based on the causality principle. This condition determines directly the velocity contrast over each interface. Using this contrast, the field in the second state can be determined, after which the next layer can be stripped by repeating the process. The imaging condition proved to give very good results for 1D and 2D-horizontally layered media. A comparison to a Schur-based layer-stripping method (which does not account for laterally varying media) proved the causality-based method to be much more stable in case of noise.

KEY WORDS:

Reciprocity theorem, imaging condition, layer-stripping

INTRODUCTION

When an imaging procedure is to be satisfactorily applied to 4D-seismic exploration it is required to be both very precise and able to deal with laterally variant media. So far, accurate imaging procedures based on the layer-stripping method have been derived for laterally homogeneous media only, like Yagle and Levy (1983). A technique for inhomogeneous media was proposed by Fokkema et al. (1998). This technique required a background velocity model. The method proposed here has the same physical background as explained by Fokkema et al. (1998) but does not need background velocity information. First, the basic equations for the general 3D-case are derived. The horizontally layered case is a simplification of these equations. In the following section the derivation of the causality-based imaging condition is shown. After this an explanation of the implementation procedure is given. The next section contains some results for the horizontally layered case. Numerical tests were done for several angles of incidence. Finally, a comparison was made to a method based on the Schur algorithm, showing the advantage of the causality-based method.

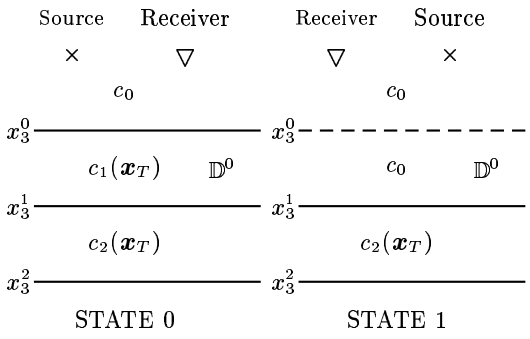

Fig. 1: Configuration of the two states in Rayleigh's reciprocity theorem.

DERIVATION OF BASIC EQUATIONS

In a three-dimensional medium with constant density, two states are defined as shown in Figure 1. The medium is divided in thin layers in which the wavespeed is assumed to vary in the lateral direction only. State 0 is the actual state, in state 1 the top layer is replaced by a layer with background medium wavespeed c_0. Application of Rayleigh's reciprocity theorem in the Laplace domain (Fokkema and van den Berg, 1993) to these states leads to:

$$\int_{\boldsymbol{x}\in\mathbb{D}^0} s^2 K(\boldsymbol{x}_T)\hat{P}^0(\boldsymbol{x}|\boldsymbol{x}^S)\hat{P}^1(\boldsymbol{x}|\boldsymbol{x}^R)\mathrm{dV} = \hat{W}[\hat{P}^0(\boldsymbol{x}^R|\boldsymbol{x}^S) - \hat{P}^1(\boldsymbol{x}^S|\boldsymbol{x}^R)], \quad (1)$$

where for simplicity of notation the dependence on the Laplace parameter $s = j\omega$ is omitted. $\boldsymbol{x}_T$ is the transverse position vector in the x_1, x_2 direction, and $\boldsymbol{x} = (\boldsymbol{x}_T, x_3)$. $\hat{W}$ is the spectrum of the source function and the contrast

function K is defined as:

$$K(\boldsymbol{x}_T) = \frac{1}{c_0^2} - \frac{1}{c_1^2(\boldsymbol{x}_T)}. \tag{2}$$

The total wavefields in state 0 and state 1 are denoted by $\hat{P}^0$ and $\hat{P}^1$, respectively. Eq. (1) is rewritten, using Parseval's theorem:

$$\begin{aligned}\frac{1}{(2\pi)^2}\int_{s\boldsymbol{\alpha}_T\epsilon\mathbb{R}^2} \mathrm{dA}\int_{x_3^0}^{x_3^1} \bar{P}^1(-js\boldsymbol{\alpha}_T, x_3|\boldsymbol{x}^R)\times \\ s^2\mathcal{K}(js\boldsymbol{\alpha}_T)\bar{P}^0(js\boldsymbol{\alpha}_T, x_3|\boldsymbol{x}^S)\mathrm{d}x_3 \\ = \hat{W}[\hat{P}^0(\boldsymbol{x}^R|\boldsymbol{x}^S) - \hat{P}^1(\boldsymbol{x}^S|\boldsymbol{x}^R)].\end{aligned} \tag{3}$$

The spatial Fourier transformation is defined as:

$$\bar{P}(js\boldsymbol{\alpha}_T, x_3|\boldsymbol{x}^S) = \int_{\boldsymbol{x}_T\epsilon\mathbb{R}^2} \exp(js\boldsymbol{\alpha}_T\cdot\boldsymbol{x}_T)\hat{P}(\boldsymbol{x}|\boldsymbol{x}^S)\mathrm{dA}. \tag{4}$$

The operation $\mathcal{K}\bar{P}^0$ is a compact way of writing the convolution in the transformed domain:

$$\begin{aligned}&\mathcal{K}(js\boldsymbol{\alpha}_T)\bar{P}^0(js\boldsymbol{\alpha}_T, x_3|\boldsymbol{x}^S) = \\ &\frac{1}{(2\pi)^2}\int_{s\boldsymbol{\alpha}'_T\epsilon\mathbb{R}^2} \bar{K}(js\boldsymbol{\alpha}_T - js\boldsymbol{\alpha}'_T)\bar{P}^0(js\boldsymbol{\alpha}'_T, x_3|\boldsymbol{x}^S)\mathrm{dA}.\end{aligned} \tag{5}$$

Now applying the operator

$$\int_{\boldsymbol{x}_T^R\epsilon\mathbb{R}^2}\exp(js\boldsymbol{\alpha}_T^R\cdot\boldsymbol{x}_T^R)\int_{\boldsymbol{x}_T^S\epsilon\mathbb{R}^2}\exp(-js\boldsymbol{\alpha}_T^S\cdot\boldsymbol{x}_T^S)\mathrm{dAdA}, \tag{6}$$

as well as the physical reciprocity property

$$\bar{\bar{P}}^1(-js\boldsymbol{\alpha}_T^S, x_3^S|js\boldsymbol{\alpha}_T^R, x_3^R) = \bar{\bar{P}}^1(js\boldsymbol{\alpha}_T^R, x_3^R| - js\boldsymbol{\alpha}_T^S, x_3^S), \tag{7}$$

to Eq. (3), we find:

$$\begin{aligned}&\frac{1}{(2\pi)^2}\int_{s\boldsymbol{\alpha}_T\epsilon\mathbb{R}^2}\mathrm{dA}\int_{x_3^0}^{x_3^1}\bar{\bar{P}}^1(js\boldsymbol{\alpha}_T^R, x_3^R| - js\boldsymbol{\alpha}_T, x_3)\times \\ &\qquad s^2\mathcal{K}(js\boldsymbol{\alpha}_T)\bar{\bar{P}}^0(js\boldsymbol{\alpha}_T, x_3| - js\boldsymbol{\alpha}_T^S, x_3^S)\mathrm{d}x_3 \\ &= \hat{W}[\bar{\bar{P}}^0(js\boldsymbol{\alpha}_T^R, x_3^R| - js\boldsymbol{\alpha}_T^S, x_3^S) \\ &\qquad -\bar{\bar{P}}^1(js\boldsymbol{\alpha}_T^R, x_3^R| - js\boldsymbol{\alpha}_T^S, x_3^S)],\end{aligned} \tag{8}$$

where $\bar{\bar{P}}$ is the wavefield in the double spatial Fourier domain, transformed with respect to the source and receiver coordinates. The total wavefield P^0 can be decomposed into an upgoing ($P^{0,r}$) and downgoing ($P^{0,i}$) part for $x_3^R \le x_3^0$. This can also be done for P^1 when $x_3^R \le x_3^1$. The incident wavefield in state 0 is known to be:

$$\begin{aligned}&\bar{\bar{P}}^{0,i}(js\boldsymbol{\alpha}_T^R, x_3^R| - js\boldsymbol{\alpha}_T^S, x_3^S) \\ &\quad = (2\pi)^2\frac{\hat{W}}{2s\Gamma_0^S}\delta(s\boldsymbol{\alpha}_T^R - s\boldsymbol{\alpha}_T^S)\exp(-s\Gamma_0^S|x_3^R - x_3^S|),\end{aligned} \tag{9}$$

with the vertical wavenumber Γ_0^S:

$$\Gamma_0^S = (\frac{1}{c_0^2} + \boldsymbol{\alpha}_T^S\cdot\boldsymbol{\alpha}_T^S)^{1/2}. \qquad \mathrm{Re}\{\Gamma_0^S\} \ge 0. \tag{10}$$

The incident field in state 1 is the same, only for reversed source and receiver positions. The reflected field in state 0 at depth x_3^R can be extrapolated from the wavefield at depth x_3^0:

$$\begin{aligned}&\bar{\bar{P}}^{0,r}(js\boldsymbol{\alpha}_T^R, x_3^R| - js\boldsymbol{\alpha}_T^S, x_3^S) = \\ &\exp(s\Gamma_0^R(x_3^R - x_3^0))\bar{\bar{P}}^{0,r}(js\boldsymbol{\alpha}_T^R, x_3^0| - js\boldsymbol{\alpha}_T^S, x_3^S), \\ &\qquad\qquad x_3^R \le x_3^0,\end{aligned} \tag{11}$$

with the vertical wavenumber Γ_0^R:

$$\Gamma_0^R = (\frac{1}{c_0^2} + \boldsymbol{\alpha}_T^R\cdot\boldsymbol{\alpha}_T^R)^{1/2}, \qquad \mathrm{Re}\{\Gamma_0^R\} \ge 0. \tag{12}$$

Analogous to Eq.(12) the reflected wavefield in state 1 can be described as:

$$\begin{aligned}&\bar{\bar{P}}^{1,r}(js\boldsymbol{\alpha}_T^R, x_3^R| - js\boldsymbol{\alpha}_T^S, x_3^S) = \\ &\exp(s\Gamma_0^R(x_3^R - x_3^1))\bar{\bar{P}}^{1,r}(js\boldsymbol{\alpha}_T^R, x_3^1| - js\boldsymbol{\alpha}_T^S, x_3^S), \\ &\qquad\qquad x_3^R \le x_3^1.\end{aligned} \tag{13}$$

Using Eq. (10) and taking for the receiver position the first interface, $x_3^R = x_3^0$, we find:

$$\begin{aligned}&s^2\hat{W}\mathcal{K}(js\boldsymbol{\alpha}_T^R)\int_{x_3^0}^{x_3^1}\frac{\exp(-s\Gamma_0^R(x_3 - x_3^0))}{2s\Gamma_0^R}\times \\ &\qquad\qquad \bar{\bar{P}}^0(js\boldsymbol{\alpha}_T^R, x_3| - js\boldsymbol{\alpha}_T^S, x_3^S)\mathrm{d}x_3 \\ &+\frac{\exp(-s\Gamma_0^R\Delta x_3)}{(2\pi)^2}\int_{s\boldsymbol{\alpha}_T\epsilon\mathbb{R}^2}\bar{\bar{P}}^{1,r}(js\boldsymbol{\alpha}_T^R, x_3^1| - js\boldsymbol{\alpha}_T, x_3^S)\mathrm{dA} \\ &\times s^2\mathcal{K}(js\boldsymbol{\alpha}_T)\int_{x_3^0}^{x_3^1}\exp(s\Gamma_0(x_3 - x_3^S))\times \\ &\qquad\qquad \bar{\bar{P}}^0(js\boldsymbol{\alpha}_T, x_3| - js\boldsymbol{\alpha}_T^S, x_3^S)\mathrm{d}x_3 \\ &= \hat{W}[\bar{\bar{P}}^{0,r}(js\boldsymbol{\alpha}_T^R, x_3^0| - js\boldsymbol{\alpha}_T^S, x_3^S) \\ &\qquad -\bar{\bar{P}}^{1,r}(js\boldsymbol{\alpha}_T^R, x_3^1| - js\boldsymbol{\alpha}_T^S, x_3^S)\exp(-s\Gamma_0^R\Delta x_3)],\end{aligned} \tag{14}$$

with

$$\Gamma_0 = (\frac{1}{c_0^2} + \boldsymbol{\alpha}_T\cdot\boldsymbol{\alpha}_T)^{1/2}, \qquad \mathrm{Re}\{\Gamma_0\} \ge 0, \tag{15}$$

and $\Delta x_3 = x_3^1 - x_3^0$. Note that the incident fields for state 0 and state 1 cancel since they are exactly the same for this receiver position. Eq. (14) is the first of our basic equations, the extrapolation equation. From this equation the upgoing wavefield in state 1, $\bar{\bar{P}}^{1,r}(js\boldsymbol{\alpha}_T^R, x_3^1| - js\boldsymbol{\alpha}_T, x_3^S)$ is calculated. When the choice for the receiver position is $x_3^R = x_3^1$, a term results in which the incident fields do not cancel. Subtracting Eq. (14), multiplied by

$\exp(s\Gamma_0^R \Delta x_3)$, from this term results in our second basic equation:

$$\begin{aligned}\bar{\bar{P}}^0(js\boldsymbol{\alpha}_T^R, x_3^1| - js\boldsymbol{\alpha}_T^S, x_3^S) = \\ \bar{\bar{P}}^{0,r}(js\boldsymbol{\alpha}_T^R, x_3^0| - js\boldsymbol{\alpha}_T^S, x_3^S)\exp(s\Gamma_0^R \Delta x_3) \\ +\bar{\bar{P}}^{0,i}(js\boldsymbol{\alpha}_T^R, x_3^0| - js\boldsymbol{\alpha}_T^S, x_3^S)\exp(-s\Gamma_0^R \Delta x_3) \\ +s^2\mathcal{K}(js\boldsymbol{\alpha}_T^R)\int_{x_3^0}^{x_3^1} \frac{\sinh(s\Gamma_0^R(x_3 - x_3^1))}{s\Gamma_0^R} \times \\ \bar{\bar{P}}^0(js\boldsymbol{\alpha}_T^R, x_3| - js\boldsymbol{\alpha}_T^S, x_3^S)\mathrm{d}x_3.\end{aligned} \quad (16)$$

From this equation the total field in state 0, $\bar{\bar{P}}^0(js\boldsymbol{\alpha}_T^R, x_3| - js\boldsymbol{\alpha}_T^S, x_3^S)$, is calculated, which is needed to be able to solve Eq. (14). Fokkema et al. (1998) proposed to solve the surface integral in Eq. (14) by a Neumann expansion.

DERIVATION OF IMAGING CONDITION

The imaging condition will be used to determine the contrast over the interface between the background medium and the layer which is about to be stripped. It is applied to the fields in state 1 that were calculated using the two basic equations, Eqs. (14) and (16), after extrapolation of the source and receiver to the interface level. The fields in this configuration will form the fields in state 0 for the next layer-stripping step. The contrast determined using the imaging condition will then be used to calculate the fields in the new state 1. In the following, the state indication will be omitted. For the derivation of the imaging condition we assume

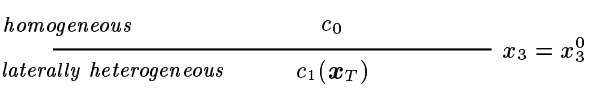

Fig. 2: Configuration for derivation of imaging condition.

a configuration as shown in Fig. 2, where the upper half-space is homogeneous, and the lower half-space is variant in the lateral direction only. This means that below the interface there are only downgoing waves. The two boundary conditions on the interface are continuity of the pressure wavefield and continuity of the particle velocity, the latter being expressed by:

$$\partial_3^{\uparrow} P\big|_{x_3^0} = \partial_3^{\downarrow} P\big|_{x_3^0}. \quad (17)$$

Since the $\boldsymbol{i}_3$-direction is downwards, $\partial_3^{\uparrow}$ represents the derivative in the homogeneous part of the medium, just above the interface, and $\partial_3^{\downarrow}$ represents the derivative just below the interface. It is also known that:

$$\partial_3^{\uparrow} \bar{\bar{P}}\big|_{x_3^0} = s\Gamma_0(\bar{\bar{P}}^r - \bar{\bar{P}}^i), \quad (18)$$

$$\bar{\bar{P}} = \bar{\bar{P}}^i + \bar{\bar{P}}^r. \quad (19)$$

In Fokkema et al. (1998) it was shown that the pressure wavefield shows a jump over the interface that is proportional to the contrast over this interface:

$$\{(\partial_3^{\uparrow})^2 - (\partial_3^{\downarrow})^2\}\bar{\bar{P}} = s^2\mathcal{K}\bar{\bar{P}}. \quad (20)$$

Note that $\mathcal{K}$ is a convolutional operator. This equation can be rewritten as:

$$(\partial_3^{\downarrow})^2\bar{\bar{P}} = (\partial_3^{\uparrow})^2\bar{\bar{P}} - s^2\mathcal{K}\bar{\bar{P}}, \quad (21)$$

and using $(\partial_3^{\uparrow})^2\bar{\bar{P}} = s^2(\Gamma_0^R)^2\bar{\bar{P}}$ as:

$$\begin{aligned}(\partial_3^{\downarrow})^2\bar{\bar{P}} &= s^2((\Gamma_0^R)^2 - \mathcal{K})\bar{\bar{P}}, \\ (\partial_3^{\downarrow})\bar{\bar{P}} &= -s\sqrt{(\Gamma_0^R)^2 - \mathcal{K}}\bar{\bar{P}}.\end{aligned} \quad (22)$$

Note that the term $\sqrt{(\Gamma_0^R)^2 - \mathcal{K}}$ is a pseudo-differential operator.

Substituting Eq. (18), and using Eq. (17):

$$\Gamma_0^R(\bar{\bar{P}}^r - \bar{\bar{P}}^i) = -\sqrt{(\Gamma_0^R)^2 - \mathcal{K}}\bar{\bar{P}}. \quad (23)$$

Now multiply Eq. (19) by Γ_0^R:

$$\Gamma_0^R\bar{\bar{P}}^r + \Gamma_0^R\bar{\bar{P}}^i = \Gamma_0^R\bar{\bar{P}}, \quad (24)$$

and add the last two equations:

$$2\Gamma_0^R\bar{\bar{P}}^r = (-\sqrt{(\Gamma_0^R)^2 - \mathcal{K}} + \Gamma_0^R)\bar{\bar{P}}. \quad (25)$$

Subtracting the same two equations results in:

$$2\Gamma_0^R\bar{\bar{P}}^i = (\sqrt{(\Gamma_0^R)^2 - \mathcal{K}} + \Gamma_0^R)\bar{\bar{P}}. \quad (26)$$

The inner product is defined as:

$$\langle\bar{\bar{f}}, \bar{\bar{g}}\rangle = \frac{1}{(2\pi)^2}\int_{-\infty}^{\infty}\bar{\bar{f}}(\boldsymbol{\alpha}_T^R)\bar{\bar{g}}(-\boldsymbol{\alpha}_T^R)\mathrm{d}\boldsymbol{\alpha}_T^R. \quad (27)$$

Now write, using $\langle\bar{\bar{f}}, \bar{\bar{g}}\rangle = \langle\bar{\bar{g}}, \bar{\bar{f}}\rangle$:

$$\begin{aligned}\langle 2\Gamma_0^R\bar{\bar{P}}^r, 2\Gamma_0^R\bar{\bar{P}}^i\rangle = 4\langle\Gamma_0^R\bar{\bar{P}}^r, \Gamma_0^R\bar{\bar{P}}^i\rangle = \\ [\langle\Gamma_0^R\bar{\bar{P}}, \Gamma_0^R\bar{\bar{P}}\rangle - \langle\Gamma_0^R\bar{\bar{P}}, \sqrt{(\Gamma_0^R)^2 - \mathcal{K}}\bar{\bar{P}}\rangle + \\ \langle\Gamma_0^R\bar{\bar{P}}, \sqrt{(\Gamma_0^R)^2 - \mathcal{K}}\bar{\bar{P}}\rangle - \\ \langle\sqrt{(\Gamma_0^R)^2 - \mathcal{K}}\bar{\bar{P}}, \sqrt{(\Gamma_0^R)^2 - \mathcal{K}}\bar{\bar{P}}\rangle] = \\ \left[\langle\Gamma_0^R\bar{\bar{P}}, \Gamma_0^R, \bar{\bar{P}}\rangle - \langle\sqrt{(\Gamma_0^R)^2 - \mathcal{K}}\bar{\bar{P}}, \sqrt{(\Gamma_0^R)^2 - \mathcal{K}}\bar{\bar{P}}\rangle\right] = \\ \left[\langle\bar{\bar{P}}, (\Gamma_0^R)^2\bar{\bar{P}}\rangle - \langle\bar{\bar{P}}, ((\Gamma_0^R)^2 - \mathcal{K})\bar{\bar{P}}\rangle\right] = \langle\bar{\bar{P}}, \mathcal{K}\bar{\bar{P}}\rangle,\end{aligned} \quad (28)$$

where we used the fact that the pseudo-differential operator $\sqrt{(\Gamma_0^R)^2 - \mathcal{K}}$ is a symmetric operator, which follows

from the symmetry of the square-root operator in the space domain (Wapenaar and Grimbergen, 1996). Now we return to a configuration with a lower halfspace that is heterogeneous in both vertical and horizontal direction. This means that the wavefield below the interface consists of both up- and downgoing waves. Due to causality, the upgoing part will always need a lapse of time to arrive at the interface. For this reason the imaging condition derived above is still valid, but only at times very close to $t = 0$. This also explains the recursive character of the procedure; each interface has to be analysed separately at time $t = 0$. We now write for the imaging condition:

$$\mathcal{F}^{-1}[4\langle \Gamma_0^R \bar{\bar{P}}^r, \Gamma_0^R \bar{\bar{P}}^i \rangle] = \mathcal{F}^{-1}[\langle \bar{\bar{P}}, \mathcal{K}\bar{\bar{P}} \rangle], \qquad t = 0, \quad (29)$$

where $\mathcal{F}^{-1}$ stands for the inverse temporal Fourier transform. The inner products are calculated in the frequency domain, after which they are transformed back to the time domain, and the contrast is determined for time $t = 0$. The application of the imaging condition, which directly determines the contrast over an interface, is what makes this procedure different from other imaging procedures.

2-D HORIZONTALLY LAYERED CASE

In the case of a two-dimensional horizontally layered medium, the convolutional operator $\mathcal{K}$ becomes a scalar K. Also the surface integral vanishes. The basic equations in this case are:

$$\begin{aligned} & s^2 K \hat{W} \int_{x_3^0}^{x_3^1} \frac{\exp(-s\gamma_0^R(x_3 - x_3^0))}{2s\gamma_0^R} \bar{P}^0(js\alpha_1^R, x_3|x_3^S)\mathrm{d}x_3 \\ & + \exp(-s\gamma_0^R \Delta x_3)\bar{P}^{1,r}(js\alpha_1^R, x_3^1|x_3^S) \times \\ & s^2 K \int_{x_3^0}^{x_3^1} \exp(s\gamma_0(x_3 - x_3^S))\bar{P}^0(js\alpha_1, x_3|x_3^S)\mathrm{d}x_3 \\ & = \hat{W}[\bar{P}^{0,r}(js\alpha_1^R, x_3^0|x_3^S) \\ & \qquad - \bar{P}^{1,r}(js\alpha_1^R, x_3^1|x_3^S)\exp(-s\gamma_0^R \Delta x_3)], \end{aligned} \quad (30)$$

and:

$$\begin{aligned} & \bar{P}^0(js\alpha_1^R, x_3^1|x_3^S) = \\ & \quad \bar{P}^{0,r}(js\alpha_1^R, x_3^0|x_3^S)\exp(s\gamma_0^R \Delta x_3) + \\ & \quad \bar{P}^{0,i}(js\alpha_1^R, x_3^0|x_3^S)\exp(-s\gamma_0^R \Delta x_3) \\ & \quad + s^2 K \int_{x_3^0}^{x_3^1} \frac{\sinh(s\gamma_0^R(x_3 - x_3^1))}{s\gamma_0^R} \bar{P}^0(js\alpha_1^R, x_3|x_3^S)\mathrm{d}x_3, \end{aligned} \quad (31)$$

where:

$$\gamma_0^R = (\frac{1}{c_0^2} + (\alpha_1^R)^2)^{1/2}, \qquad \mathrm{Re}\{\gamma_0\} \geq 0. \quad (32)$$

The imaging condition in case of a horizontally layered two-dimensional medium takes the following form:

$$\mathcal{F}^{-1}[\gamma^2 \hat{P}^r \hat{P}^i] = \frac{1}{4} K \times \mathcal{F}^{-1}[\hat{P}^2], \qquad t = 0, \quad (33)$$

where $\mathcal{F}^{-1}$ stands for the inverse temporal Fourier transform.

IMPLEMENTATION

The layer-stripping procedure is as follows: Pressure and velocity data are collected on the interface between the two halfspaces. The data can be decomposed in an upgoing and downgoing pressure field following (Fokkema and van den Berg, 1993). The imaging condition is applied to the first interface, such that the contrast over this interface can be determined. Using this contrast, the field in state 0 at level x_3^1 can be determined by applying Eq. (16). After this, Eq. (14) is used to determine the upgoing field in state 1. The source and receiver positions are now extrapolated to level x_3^1. State 1 will now become our new state 0 and the next layer will be stripped by repeating the procedure, as shown below:

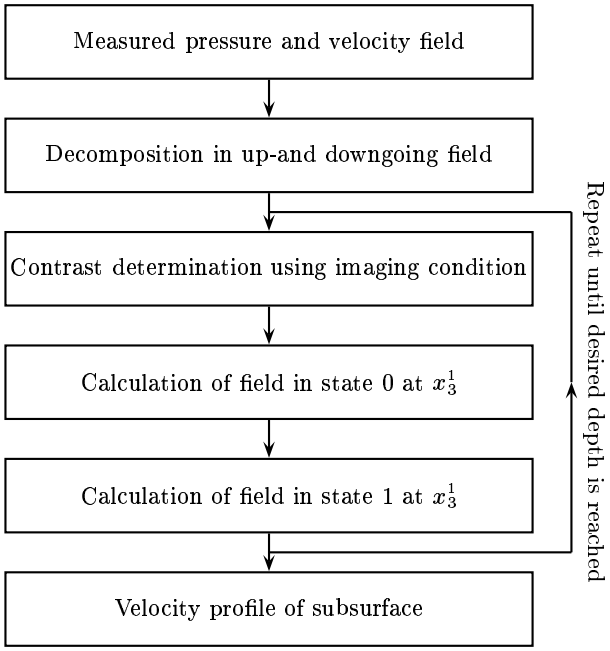

Fig. 3: Flow diagram of layer-stripping algorithm.

SOME RESULTS

To test the algorithm, some experiments were done for a one-dimensional medium with two interfaces, one at a depth of 150 m and one at a depth of 300 m. The velocity of the background medium is 1500 m/s, of the first layer 2000 m/s, and of the second layer 4000 m/s. Synthetic data were generated using a modeling program based on the recursion formula (Fokkema and Ziolkowski, 1987). The velocity model is shown in Figure 4 together with the velocities determined by the layer-stripping procedure.

The thickness of the stripped layers is 1.5 m. For the

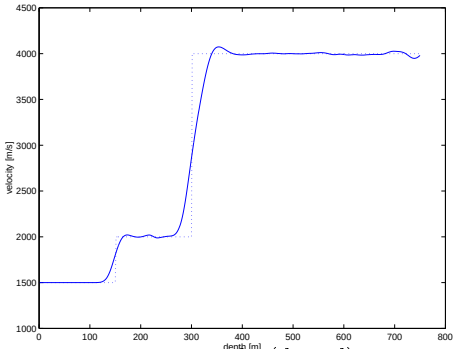

Fig. 4: Three layer velocity model (dashed) together with the calculated velocities (solid).

wavelet a zero-phase Gaussian was used. Instead of using just the value of the wavefields at time $t = 0$ when applying the imaging condition, the energy of the wavelet around time $t = 0$ was used. The results are very close to the modeled velocities. Figure 5 shows the calculated upgoing field in state 1 after every 20 layer-stripping steps. The upper trace is the syntheticly generated trace. Obviously, the primary reflection moves closer to time $t = 0$ when the medium is penetrated deeper. When the first reflection reaches time $t = 0$ it is 'detected' by the algorithm, and the contrast gets a value while the second reflection keeps moving to the $t = 0$-axis, now with a different speed. The multiple reflection, which is hardly visible in the figure due to the scale, travels with double speed towards time $t = 0$ and reaches this point exactly together with the primary reflection that caused it. The procedure handles the multiples in the data correctly. In Eq. (14) a multiple generator term can be recognized (van Borselen, 1995).

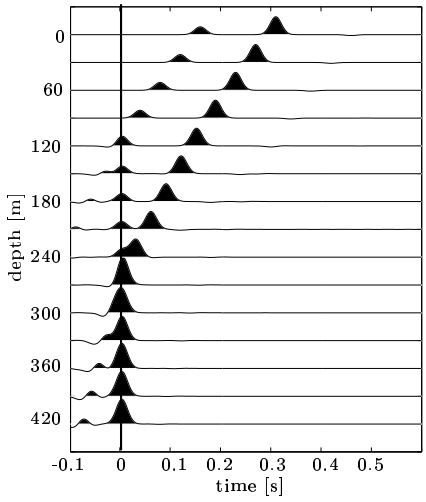

Fig. 5: Calculated reflected field in state 1 for every 20 layer-stripping steps.

Figure 6 shows velocity results for a more complicated earth model (the Amsterdam model). The results for this model are still satisfactory. The overshoot or 'ears' near the velocity jumps are a results of the Gibb's phenomenon and can easily removed by a filter, as shown in Fig. 7. Tests on horizontally layered media also proved good results for different angles of incidence. This is shown in Fig. 8 for two different p-values, where $p = \sin\phi/c_0$. A known problem with existing layer-stripping methods is the accumulation of errors during the process. To test the sensitivity of our causality-based method to these kind of errors, it was compared to a Schur-based layer-stripping method (Yagle and Levy, 1983). This method already shows more deviation from the original model for clean data, as shown in Fig. 9. Note that the highest values in this figure are much higher than the model values. An example for rather heavily disturbed data is shown in Figs. 10 and 11, where the causality-based method shows much better results than the Schur method.

CONCLUSIONS

The theory of a layer-stripping method for laterally varying media was derived. This method makes use of an imaging method which is based on the causality principle, which yields directly the contrast parameters of the medium. Testing for horizontally layered media shows good results. The laterally varying case involves solving convolutional and pseudo-differential operators. This is what our current work focuses on, as well as on the application of this algorithm to time-lapse problems.

REFERENCES

Fokkema, J. T., and van den Berg, P. M., 1993, Seismic applications of acoustic reciprocity: Elsevier.

Fokkema, J. T., and Ziolkowski, A., 1987, The critical reflection theorem: Geophysics, **52**, no. 7, 965–972.

Fokkema, J. T., Smit, R., and Wapenaar, C. P. A., 1998, Velocity replacement techniques in inhomogeneous media:, *in* Delphi Consortium 9.

van Borselen, R. G., 1995, Removal of surface-related multiples from marine seismic data: Ph. D.thesis, Delft University of Technology, The Netherlands.

Wapenaar, C. P. A., and Grimbergen, J. L. T., 1996, Reciprocity theorems for one-way wavefields: Geophys. J. int, **127**, 169–177.

Yagle, A. E., and Levy, B. C., 1983, Application of the schur algorithm tot the inverse prolem for a layered acoustic medium: J. Acoust. Soc. Am., **76**, 301–308.

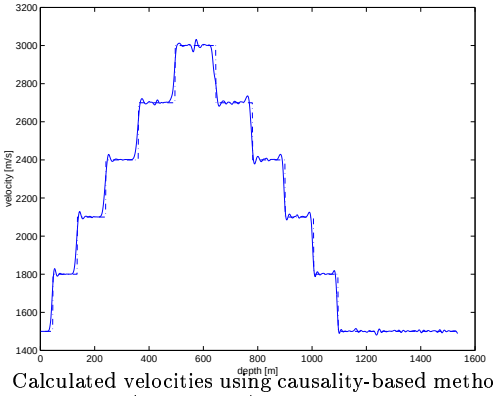

Fig. 6: Calculated velocities using causality-based method and the velocity model (dashed line).

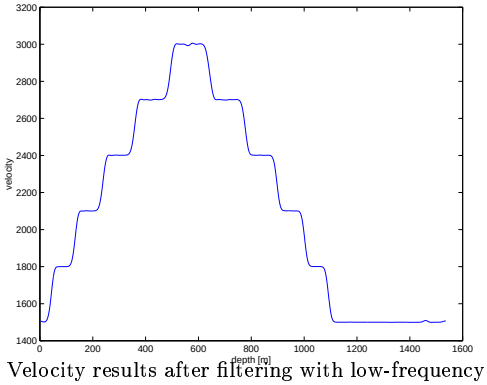

Fig. 7: Velocity results after filtering with low-frequency filter.

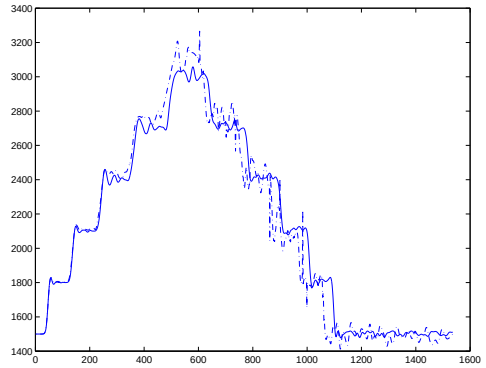

Fig. 8: Calculated velocities for waves at oblique incidence (p=2e-4 (solid) and p=3e-4 (dashed).)

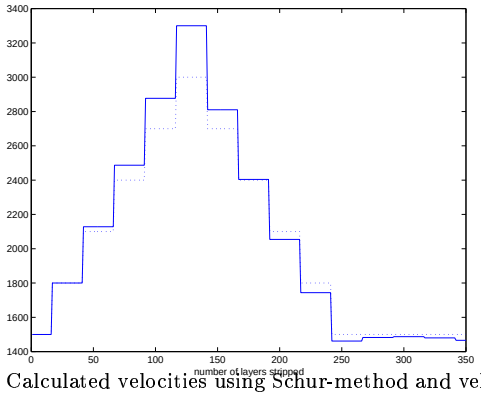

Fig. 9: Calculated velocities using Schur-method and velocity model (dashed line).

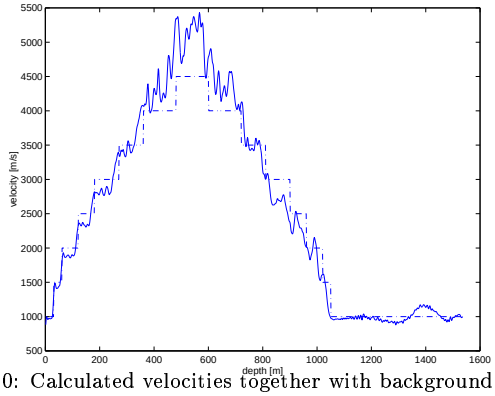

Fig. 10: Calculated velocities together with background model. The data was disturbed with noise.

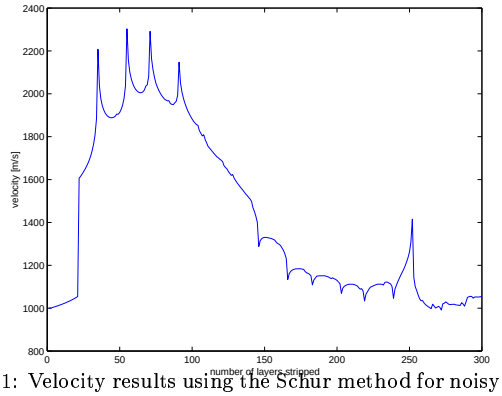

Fig. 11: Velocity results using the Schur method for noisy data.